# Scale and Boundary Conditions Effects on the Apparent Elastic Moduli of Trabecular Bone Modeled as a Periodic Cellular Solid

**Congyu Wang**
Department of Mechanical and Industrial Engineering,
Concordia University,
Montreal, QC, H3G 1M8, Canada
e-mail: wangcongyu@hotmail.com

**Liang Feng**
e-mail: lfeng4@illinois.edu

**Iwona Jasiuk**
e-mail: ijasiuk@illinois.edu

Department of Mechanical Science and Engineering,
University of Illinois at Urbana-Champaign,
Urbana, IL 61801

*We study apparent elastic moduli of trabecular bone, which is represented, for simplicity, by a two- or three-dimensional periodic cellular network. The term "apparent" refers to the case when the region used in calculations (or specimen size) is smaller than a representative volume element and the moduli depend on the size of that region and boundary conditions. Both the bone tissue forming the network and the pores (represented by a very soft material) are assumed, for simplicity, as homogeneous, linear elastic, and isotropic. In order to investigate the effects of scale and boundary conditions on the moduli of these networks we vary the specimen size and apply four different boundary conditions: displacement, traction, mixed, and periodic. The analysis using periodic boundary conditions gives the effective moduli, while the displacement, traction, and mixed boundary conditions give apparent moduli. The apparent moduli calculated using displacement and traction boundary conditions bound the effective moduli from above and below, respectively. The larger is the size of the region used in our calculations, the closer are the bounds. Our choice of mixed boundary conditions gives results that are very close to those obtained using periodic boundary conditions. We conduct this analysis computationally using a finite element method. We also investigate the effect of mismatch in elastic moduli of bone tissue and soft fill, trabecular bone structure geometry, and bone tissue volume fraction on the apparent elastic moduli of idealized periodic models of trabecular bone. This study gives guidance on how the size of the specimen and boundary conditions (used in experiments or simulations) influence elastic moduli of cellular materials. This approach is applicable to heterogeneous materials in general.*
[DOI: 10.1115/1.4000192]

*Keywords: apparent elastic moduli, trabecular bone, scale and boundary conditions effects, representative volume element, periodic microstructure*

## 1 Introduction

The trabecular bone has a porous structure made of a highly irregular network of struts and plates (Fig. 1(*a*)). Such a complex architecture poses numerous challenges from the analysis viewpoint. A number of researchers addressing the overall properties of the trabecular bone accounted for the actual structure of bone by importing micro-computed tomography (micro-CT) images of bone samples to finite element models (e.g., Refs. [1–8]). A simulated random model of trabecular bone, involving a Voronoi network, was used by Silva et al. [9,10] to study the effect of geometrical factors, such as thinning of walls and a random removal of struts, on mechanical properties of bone.

Other studies employed various idealized periodic models of trabecular bone structure. Analytical studies of regular cellular structures, including those applicable to trabecular bone, are due to Ashby [11], Gibson and co-worker [12,13], Christensen [14], and others. Numerical analyses of periodic models of trabecular bone involving a finite element method are due to Williams and Lewis [15], Beaupre and Hayes [16], Hollister et al. [17,1], Guo et al. [18], Werner et al. [19], Kowalczyk [20], and others. Several computational studies represented bone as a generalized continuum using a Cosserat (or couple stress) theory [21–27]. These works were motivated by the experimental studies of Lakes and co-workers [28–32], which showed Cosserat effects in bone.

All the above mentioned papers assumed that the bone tissue was linear elastic and isotropic. Fewer theoretical studies accounted for viscoelastic (e.g., Ref. [33]) and poroelastic (e.g., Ref. [34]) properties of bone tissue. Anisotropy of bone tissue is also neglected, in general, with focus being paid on the architectural anisotropy of trabecular bone (e.g., Refs. [35–37]). Also, bone is spatially inhomogeneous (e.g., Refs. [38,39]), which may have appreciable effects on trabecular bone modulus if spatial variations in tissue modulus are large. In this paper we assume, for simplicity, that bone tissue is homogeneous, linear elastic, and isotropic.

A fundamental question in predicting the effective properties of trabecular bone, or any other material with microstructure, is how large of a region to use in calculations or testing so that the boundary conditions effects are minimized. To address this issue the concept of a representative volume element (RVE) was introduced [40,41]. The RVE is a region much smaller than the size of a whole composite structure but much larger than the size of microstructural features (diameter of pores, for example), it has the same properties as a whole composite, and the properties do not depend on boundary conditions. In words of Hill [41], the RVE is "structurally entirely typical of the whole mixture on average, and

Contributed by the Bioengineering Division of ASME for publication in the JOURNAL OF BIOMECHANICAL ENGINEERING. Manuscript received August 13, 2008; final manuscript received August 26, 2009; accepted manuscript posted September 10, 2009; published online November 17, 2009. Assoc. Editor: Michael Sacks.

  

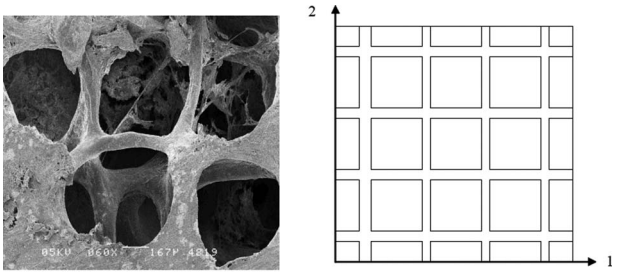


**Fig. 1 (*a*) SEM image of trabecular bone; (*b*) idealized 2D periodic model of trabecular bone**

contains a sufficient number of inclusions for the apparent overall moduli to be effectively independent of the surface values of traction and displacement, as long as these values are 'macroscopically uniform'." The RVE was further discussed in reviews and books by Hashin [42], Aboudi [43], Christensen [44], and Ostoja-Starzewski [45], among others. The first book concerning the determination of the RVE size—as opposed to the properties of the RVE only—is Microstructural Randomness and Scaling in Mechanics of Materials [46]; see also references therein.

The trabecular bone has finite dimensions and a spatially changing porosity, so the amount of tissue available for testing is limited. Due to these reasons and computational simplicity, only small trabecular bone regions are generally used for testing or computations. Thus, the material sample window of the trabecular bone is smaller than the RVE, which results in obtaining the *apparent* properties, as opposed to effective properties, experimentally or computationally. These apparent properties are dependent on the size of the specimen (or region used in computations) and boundary conditions, creating a hierarchy of material bounds [47]

$$\boldsymbol{C}^R \equiv (\boldsymbol{S}^R)^{-1} \equiv \langle \boldsymbol{S}_1^t \rangle^{-1} \leq \langle \boldsymbol{S}_{\delta'}^t \rangle^{-1} \leq \langle \boldsymbol{S}_{\delta}^t \rangle^{-1} \leq \boldsymbol{C}^{\text{eff}} \leq \langle \boldsymbol{C}_{\delta}^d \rangle \leq \langle \boldsymbol{C}_{\delta'}^d \rangle \leq \langle \boldsymbol{C}_1^d \rangle \equiv \boldsymbol{C}^V \tag{1}$$

where $\forall \delta' < \delta$ and

$$\boldsymbol{C} > \boldsymbol{D} \Leftrightarrow (\boldsymbol{C} - \boldsymbol{D}){:}a{:}a > 0 \quad \text{for any tensor } a_{ij} \neq 0$$

$\boldsymbol{C}$ is the fourth order stiffness tensor $C_{ijkl}$. The superscripts $R$ and $V$ denote the Voigt and Reuss bounds, respectively, while the superscripts $t$ and $d$ refer to traction and displacement boundary conditions. Following Eq. (1), the effective properties are bound from above and below by the apparent elastic moduli obtained using displacement and traction boundary conditions, respectively. The larger is the size of the window $\delta$ (region used in experiments or computations), the closer are the bounds. When the size of the window reaches the size of the RVE, the effective properties are obtained. Also, following the works of Hazanov and co-workers [48,49]

$$(\boldsymbol{S}_{\delta}^t)^{-1} < \boldsymbol{C}_{\delta}^{dt} < \boldsymbol{C}_{\delta}^d \tag{2}$$

where the superscript $dt$ denotes mixed boundary conditions. In this paper we focus on the effects of scale (window size) and boundary conditions on the overall elastic moduli of the trabecular bone. We represent the trabecular bone using idealized two-dimensional (2D) and three-dimensional (3D) periodic models and employ a finite element method to predict the effective and apparent elastic moduli of such structures computationally.

Next, we review several fundamental concepts from micromechanics, which will be used in our analysis. The Hill condition, which guarantees that effective moduli calculated by energy and direct approaches are the same, states that the volume average of the product of stress and strain is equal to the product of the volume average of stress and the volume average of strain [41]. It is given as ma dove lo dice???

$$\overline{\sigma_{ij}\varepsilon_{ij}} = \bar{\sigma}_{ij}\bar{\varepsilon}_{ij} \tag{3}$$

where $\sigma_{ij}$ and $\varepsilon_{ij}$ are the stress and strain tensors, respectively, and the overbar denotes a volume average, integrated over the sample window $V$ (e.g., $\bar{\sigma}_{ij} = 1/V \int_V \sigma_{ij} dV$). We will use the Hill condition to check our computational results. Upon integration, Eq. (3) gives

$$\int_S (t_i - \overline{\sigma_{ij}} n_j)(u_i - \overline{\varepsilon_{ij}} x_j) dS = 0 \tag{4}$$

where $S$ is a surface of the material window. Condition (4) is satisfied for the following boundary conditions:

(a) natural (traction-controlled)

$$t_i = \sigma_{ij}^0 n_j \quad \text{on } S \tag{5}$$

(b) kinematic (displacement-controlled)

$$u_i = \varepsilon_{ij}^0 x_j \quad \text{on } S \tag{6}$$

(c) mixed

$$(t_i - \sigma_{ij}^0 n_j)(u_i - \varepsilon_{ij}^0 x_j) = 0 \quad \text{on} \quad S \tag{7}$$

where $\sigma_{ij}^0$ and $\varepsilon_{ij}^0$ are the uniform applied stress and strain, respectively. Note that in Eq. (7) only one component of $t_i$ or $u_i$ is specified at a time on a given surface. For more discussion on mixed boundary conditions, see Refs. [50,51].

In the above equations, we used the average stress theorem, which states that under traction boundary conditions (Eq. (5)), the average stress $\bar{\sigma}_{ij}$ is equal to the applied (uniform) stress $\sigma_{ij}^0$

$$\bar{\sigma}_{ij} = \sigma_{ij}^0 \tag{8}$$

and the average strain theorem, which states that under displacement boundary conditions (Eq. (6)), the average strain $\bar{\varepsilon}_{ij}$ is equal to the applied (uniform) strain $\varepsilon_{ij}^0$

$$\bar{\varepsilon}_{ij} = \varepsilon_{ij}^0 \tag{9}$$

We evaluate the effective or apparent elastic moduli of trabecular bone using an energy approach, which involves equating the elastic strain energy of the bone network (heterogeneous material) $W^{\text{cell}}$(with superscript "cell" denoting the region used for calculations, also called a window) and the elastic strain energy of the equivalent homogeneous medium $W^{\text{equiv}}$

$$W^{\text{cell}} = W^{\text{equiv}} \tag{10}$$

The elastic strain energy of the heterogeneous material (trabecular bone network) is obtained as follows:

$$W^{\text{cell}} = \frac{1}{2}\int_V \sigma_{ij}\varepsilon_{ij} dV = \frac{V}{2}\overline{\sigma_{ij}\varepsilon_{ij}} \tag{11}$$

where $V$ denotes volume of a region used for analysis.

The elastic strain energy of an equivalent elastic homogeneous material having the overall properties of trabecular bone is given as follows. When the displacement boundary conditions (Eq. (6)) (with a uniform strain $\varepsilon_{ij}^0$) are applied on the surface of an RVE, then the elastic strain energy of the equivalent homogeneous medium is given by

$$W^{\text{equiv}} = \frac{V}{2}\varepsilon_{ij}^0 C_{ijkl}^{\text{eff}} \varepsilon_{kl}^0 \tag{12}$$

using Eqs. (3) and (9), where $C_{ijkl}^{\text{eff}}$ is the effective elastic stiffness. When traction boundary conditions (Eq. (5)) (with a uniform stress $\sigma_{ij}^0$) are applied, then the elastic strain energy of the equivalent homogeneous medium is given by

$$W^{\text{equiv}} = \frac{V}{2}\sigma^0_{ij}S^{\text{eff}}_{ijkl}\sigma^0_{kl} \tag{13}$$

using Eqs. (3) and (8), where $S^{\text{eff}}_{ijkl}$ is the effective elastic compliance.

When the size of the window of observation is smaller than the RVE and displacement boundary conditions are applied, then the elastic strain energy of the equivalent homogeneous medium is given by

$$W^{\text{equiv}} = \frac{V}{2}\varepsilon^0_{ij}C^d_{ijkl}\varepsilon^0_{kl} \tag{14}$$

using Eqs. (3) and (9), where $C^d_{ijkl}$ is the apparent stiffness tensor (subscript $d$ denotes displacement boundary conditions). Equation (14) is also employed when mixed boundary conditions are used to find the apparent stiffness tensor $C^{dt}_{ijkl}$. When traction boundary conditions are applied, the elastic strain energy of the equivalent homogeneous medium is given by

$$W^{\text{equiv}} = \frac{V}{2}\sigma^0_{ij}S^t_{ijkl}\sigma^0_{kl} \tag{15}$$

where $S^t_{ijkl}$ is the apparent compliance tensor (subscript $t$ denotes traction boundary conditions).

Finally, we evaluate the effective and apparent elastic moduli of trabecular bone by equating the elastic strain energy of the heterogeneous medium $W^{\text{cell}}$ (our idealized periodic model of trabecular bone) and the elastic strain energy of the equivalent homogeneous medium $W^{\text{equiv}}$, as given by Eq. (10).

We conduct these calculations by applying four types of boundary conditions: displacement, traction, mixed, and periodic and by varying the size of a "window of observation" (region used in analysis) to obtain the scale and boundary conditions effects on the apparent elastic moduli of trabecular bone.

Several researchers also studied the effect of specimen size (or window size) and boundary conditions, experimentally and computationally, in the context of composites (e.g., Refs. [46–49,52–56]), cellular materials (e.g., Ref. [57]), and trabecular bone [58–61,17,1,62–66,51]. Our earlier works in this area focused on matrix-inclusion composites [54,67,68]. The issues addressed included the effects of periodic versus random microstructure, size of a window as compared with a dimension of microstructure, and boundary conditions on the overall materials response. The current paper extends these results to periodic cellular materials. The closely related works are due to Hollister and Kikuchi [57] who studied elastic responses of periodic porous two-dimensional composites using displacement, traction, and periodic boundary conditions, and Pahr and Zysset [51] who computed apparent properties of trabecular bone using displacement, traction, periodic, and mixed boundary conditions by considering six specimens from the human trabecular bone. They also extended mixed boundary condition formulation of Hazanov [50] to shear loading for porous materials.

## 2 Geometric Model

We model trabecular bone as an idealized 2D or 3D periodic network, as shown in Fig. 1(*b*) and evaluate its elastic constants using the finite element program ANSYS 8.1. We use solid elements (Quad 82 type) and a plane stress with thickness option. The pores are represented as squares in two dimensions or interconnected cubes in three dimensions. The walls of the structure have assigned bone tissue properties, while pores are filled with a very soft material. We choose such geometric model for computational simplicity. A similar structure was studied by Hollister et al. [17] and Adachi et al. [21], among others. We consider the periodic, as opposed to a random microstructure, also for simplicity, so we do not need to consider many realizations to obtain statistical averages.

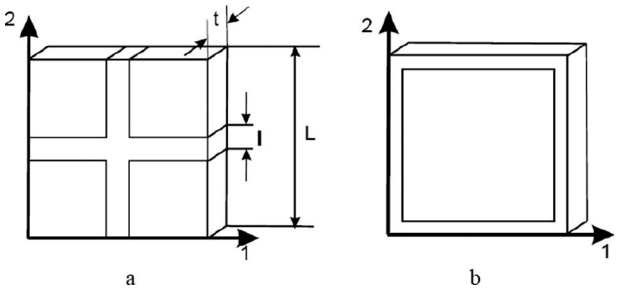


**Fig. 2 Two different units cells: (*a*) Unit cell 1 and (*b*) Unit cell 2**

Two different unit cells, shown in Fig. 2, are used in calculations. The first unit cell choice involves cutting the periodic bone structure at midpoint of bone struts, which results in both the bone tissue and the fill material being present on boundaries (Fig. 2(*a*)). The second unit cell choice involves cutting bone struts across their length (Fig. 2(*b*)), which results in an outer stiff core and an inner soft fill configuration. The geometric parameters characterizing our simplified model of trabecular bone are the bone strut thickness ($t$) and the bone strut in-plane thickness ($l$) (Fig. 2(*a*)). Three tissue volume fractions are examined: 5%, 10%, and 20%. The dimensions of the unit cell ($L\times L\times t$) shown in Fig. 2 are taken as $5\times 5\times 0.1$, which gives the in-plane thickness of the bone strut ($l$) of 0.528 for the volume fraction of 20%.

In order to study the effect of scale (or size of a window) we choose different sample sizes, involving a unit cell of dimension $\delta=\delta_0$, and larger cells, up to $\delta=6\delta_0$. Several different window sizes ($\delta_0, 2\delta_0, 3\delta_0$) are shown in Fig. 3.

**2.1 Material Inputs.** We model trabecular bone as a two phase material consisting of a bone tissue (stiff phase) forming a trabecular network and pores (soft phase) modeled by assigning very small elastic moduli. For simplicity, we assume that both phases are homogeneous, linear elastic, and isotropic. The bone tissue is assigned the Young's modulus $E_b=13.0$ GPa and the Poisson ratio $\nu_b=0.3$, while the pores (filled with very soft material) have the Young's modulus $E_s=13.0$ kPa while keeping the Poisson ratio as $\nu_s=0.3$. This gives the mismatch in elastic moduli of $E_b/E_s=10^6$. The Young modulus of bone tissue was chosen from a variety of values given in literature (e.g., Refs. [69,70]). However, since the problem is linear elastic, it is scalable so the actual value of the modulus is not important. The very small value of $E_s$, as compared with $E_b$, makes this problem equivalent to the case when the soft fill is not present, i.e., the space is represented by voids. Such assumption has been used in most computational studies on trabecular bone. We need to include in our model the fill with very small but nonzero properties to ensure that the average stress and strain theorems and the Hill condition are satisfied.

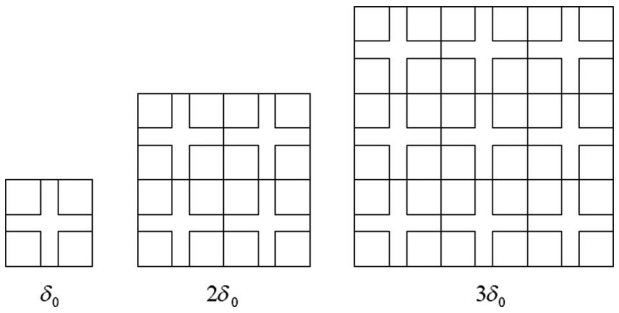


**Fig. 3 Three different window sizes $\delta_0$, $2\delta_0$ and $3\delta_0$**

## 3 Method of Solution

To investigate the effective and apparent elastic moduli of our idealized periodic model of trabecular bone, we consider different sizes of unit cells (Fig. 3) and four types of boundary conditions: displacement, traction, mixed, and periodic. Since our geometric models are effectively orthotropic with cubic symmetry, for the 2D model only the elastic stiffness components $C_{1111}=C_{2222}$, $C_{1122}=C_{2211}$, and $C_{1212}=C_{2121}$ need to be evaluated. The same observations hold for elastic compliance components. In order to determine the elastic stiffness $C_{ijkl}$, or the elastic compliance $S_{ijkl}$ components, three types of loads: uniaxial extension or tension, biaxial extension or tension, and shear deformation or shear traction, are applied. The analysis of 3D model also requires the evaluation of only three components of stiffness or compliance tensor because of cubic symmetry. Next, we discuss the boundary value problems needed to evaluate the effective and apparent elastic moduli in the context of a 2D setting. The analysis for the 3D geometry is analogous (see, e.g., Ref. [27]).

**3.1 Displacement Boundary Conditions.** When displacement boundary conditions are applied and the size of sample (cell) is smaller than the RVE, the stiffness tensor $C^d_{ijkl}$ is calculated. The subscript $d$ denotes the applied displacement boundary conditions.

*3.1.1 Uniaxial extension.* When a uniform strain $\varepsilon^0_{11}$ is applied on a sample boundary $S$, the displacement boundary conditions are

$$u_1(\underline{x}) = \varepsilon^0_{11} x_1, \quad u_2(\underline{x}) = 0 \quad \text{on} \quad S \tag{16}$$

which gives $C^d_{1111}=(2W^{\text{cell}})/V$, when $\varepsilon^0_{11}=1$ (chosen as unity for simplicity) due to symmetry $C^d_{1111}=C^d_{2222}$.

*3.1.2 Biaxial extension.* When the uniform strain $\varepsilon^0_{11}=\varepsilon^0_{22}$ is applied on the sample boundary $S$, the displacement boundary conditions are

$$u_1(\underline{x}) = \varepsilon^0_{11} x_1, \quad u_2(\underline{x}) = \varepsilon^0_{22} x_2 \quad \text{on} \quad S \tag{17}$$

which gives $C^d_{1122}=(W^{\text{cell}}/V)-C^d_{1111}$ when $\varepsilon^0_{11}=\varepsilon^0_{22}=1$. Note that the $C^d_{1111}$ test must be done first to calculate $C^d_{1122}$.

*3.1.3 Shear deformation.* When a uniform strain $\varepsilon^0_{12}=\varepsilon^0_{21}$ is applied on the sample boundary $S$, the displacement boundary conditions are written as

$$u_1(\underline{x}) = \varepsilon^0_{12} x_2, \quad u_2(\underline{x}) = \varepsilon^0_{12} x_1 \quad \text{on} \quad S \tag{18}$$

which gives $C^d_{1212}=W^{\text{cell}}/2V$ when $\varepsilon^0_{12}=\varepsilon^0_{21}=1$.

**3.2 Traction Boundary Conditions.** When traction boundary conditions are applied and the sample size is smaller than the RVE, we obtain the apparent compliance tensor $S^t_{ijkl}$ (the subscript $t$ denotes traction boundary conditions). By inverting this compliance tensor, $(S^t_{ijkl})^{-1}=C^t_{ijkl}$, the stiffness tensor $C^t_{ijkl}$ is obtained.

*3.2.1 Uniaxial tension.* When a uniform stress $\sigma^0_{11}$ is applied on the sample boundary $S$, the traction boundary condition is

$$t_1(\underline{x}) = \sigma^0_{11} n_1, \quad t_2(\underline{x}) = 0 \quad \text{on} \quad S \tag{19}$$

which gives $S^t_{1111}=2W^{\text{cell}}/V$ when $\sigma^0_{11}=1$ due to symmetry $S^t_{1111}=S^t_{2222}$.

*3.2.2 Biaxial tension.* When the uniform stress $\sigma^0_{11}=\sigma^0_{22}$ is applied on the sample boundary $S$, the traction boundary conditions are

$$t_1(\underline{x}) = \sigma^0_{11} n_1, \quad t_2(\underline{x}) = \sigma^0_{22} n_2 \quad \text{on} \quad S \tag{20}$$

which gives $S^t_{1122}=(W^{\text{cell}}/V)-S^t_{1111}$ when $\sigma^0_{11}=\sigma^0_{22}=1$. Note that again the $S^t_{1111}$ test must be done first to calculate $S^t_{1122}$.

*3.2.3 Shear traction.* When a uniform stress $\sigma^0_{12}=\sigma^0_{21}$ is applied on the sample boundary $S$, the traction boundary condition is

$$t_1(\underline{x}) = \sigma^0_{12} n_2, \quad t_2(\underline{x}) = \sigma^0_{12} n_1 \quad \text{on} \quad S \tag{21}$$

which gives $S^t_{1212}=W^{\text{cell}}/2V$ when $\sigma^0_{12}=\sigma^0_{21}=1$.

**3.3 Mixed Boundary Conditions.** Mixed boundary conditions include both traction and displacement boundary conditions applied on the sample boundary. The obtained apparent stiffness tensor is denoted by $C^{dt}_{ijkl}$. We use the following mixed boundary conditions.

*3.3.1 Mixed uniaxial extension.* When a uniform strain $\varepsilon^0_{11}$ and shear stress $\sigma^0_{12}=\sigma^0_{21}=0$ are applied on the sample's boundary, the mixed boundary conditions are written as

$$\begin{gathered} \text{on } n_1 \text{ face} \quad u_1 = \varepsilon^0_{11} x_1, \quad t_2 = \sigma^0_{12} n_1 = 0 \\ \text{on } n_2 \text{ face} \quad u_2 = 0, \quad t_1 = \sigma^0_{12} n_2 = 0 \end{gathered} \tag{22}$$

which give $C^{dt}_{1111}=2W^{\text{cell}}/V$ when $\varepsilon^0_{11}=1$.

*3.3.2 Mixed biaxial extension.* When the uniform strain $\varepsilon^0_{11}=\varepsilon^0_{22}$ and shear stress $\sigma^0_{12}=\sigma^0_{21}=0$ are applied on the sample's boundary, the mixed boundary conditions are

$$\begin{gathered} \text{on } n_1 \text{ face} \quad u_1 = \varepsilon^0_{11} x_1, \quad t_2 = \sigma^0_{12} n_1 = 0 \\ \text{on } n_2 \text{ face} \quad u_2 = \varepsilon^0_{22} x_2, \quad t_1 = \sigma^0_{12} n_2 = 0 \end{gathered} \tag{23}$$

which gives $C^{dt}_{1122}=W^{\text{cell}}/V-C^{dt}_{1111}$ when $\varepsilon^0_{11}=\varepsilon^0_{22}=1$.

*3.3.3 Mixed shear deformation.* When a uniform strain $\varepsilon^0_{12}=\varepsilon^0_{21}$ and normal stresses $\sigma^0_{11}=\sigma^0_{22}=0$ are applied on the sample's boundary, the mixed boundary conditions are

$$\begin{gathered} \text{on } n_1 \text{ face} \quad t_1 = \sigma^0_{11} n_1 = 0 \quad u_2 = \varepsilon^0_{12} x_1 \\ \text{on } n_2 \text{ face} \quad u_1 = \varepsilon^0_{12} x_1 \quad t_2 = \sigma^0_{22} n_2 = 0 \end{gathered} \tag{24}$$

which give $C^{dt}_{1212}=W^{\text{cell}}/2V$ when $\varepsilon^0_{12}=\varepsilon^0_{21}=1$.

**3.4 Periodic Boundary Conditions.** Finally, we apply periodic boundary conditions to predict the effective properties of the idealized periodic model of trabecular bone. The periodic boundary conditions are stated as follows:

$$u_i(\underline{x}+\underline{L}) = u_i(\underline{x}) + \varepsilon^0_{ij} L \underline{e}_j \tag{25}$$

$$t_i(\underline{x}+\underline{L}) = -t_i(\underline{x}) \tag{26}$$

Note that in the finite element program we only need to specify periodic condition (25) on displacements. The continuity of traction condition (26) will be satisfied automatically.

*3.4.1 Uniaxial extension.* When a uniform strain $\varepsilon^0_{11}$ is applied on the sample material boundary $S$, the periodic boundary conditions on displacements are written as

$$u_1(\underline{x}+\underline{L}) = u_1(\underline{x}) + \varepsilon^0_{11} L \underline{e}_1 \quad \text{on} \quad S \tag{27}$$

$$u_2(\underline{x}+\underline{L}) = u_2(\underline{x}) \quad \text{on} \quad S \tag{28}$$

which gives $C^{\text{eff}}_{1111}=2W^{\text{cell}}/V$ when $\varepsilon^0_{11}=1$; $\underline{e}_1$ is a unit vector and $L$ is the side length of a window (cell).

*3.4.2 Biaxial extension.* The periodic boundary conditions with the applied uniform strain $\varepsilon^0_{11}=\varepsilon^0_{22}$ are written as

$$u_1(\underline{x}+\underline{L}) = u_1(\underline{x}) + \varepsilon^0_{11} L \underline{e}_1 \quad \text{on} \quad S \tag{29}$$

$$u_2(\underline{x}+\underline{L}) = u_2(\underline{x}) + \varepsilon^0_{22} L \underline{e}_2 \quad \text{on} \quad S \tag{30}$$

which gives $C^{\text{eff}}_{1122}=(W^{\text{cell}}/V)-C^{\text{eff}}_{1111}$ when $\varepsilon^0_{11}=\varepsilon^0_{22}=1$; $\underline{e}_2$ is a unit vector in direction 2.

**Table 1 Effects of mesh size on elastic strain energy for different loadings ($E_b$=13 GPa, $E_b/E_s$=$10^6$, $\nu_b$=$\nu_s$=0.3, and bone tissue volume fraction 20%) where $\Delta W=(W-W_f)/W\times 100\%$**

| Mesh size of unit cell | No. of elements | $\Delta W$ uniaxial tension | $\Delta W$ uniaxial extension | $\Delta W$ biaxial tension | $\Delta W$ biaxial extension | $\Delta W$ shear traction | $\Delta W$ shear strain |
|---|---|---|---|---|---|---|---|
| 0.044 | 12,996 | 0.00 | 0.00 | 0.00 | 0.00 | 0.00 | 0.00 |
| 0.066 | 5776 | −0.02 | −0.85 | −0.03 | −0.86 | 0.00 | −2.24 |
| 0.088 | 3364 | −0.04 | −0.76 | −0.09 | −0.73 | 0.00 | −2.01 |
| 0.132 | 1444 | −0.11 | −0.58 | −0.25 | −0.45 | 0.00 | −1.65 |
| 0.176 | 841 | −0.20 | −0.40 | −0.40 | −0.18 | −0.28 | −1.09 |
| 0.264 | 400 | −0.05 | −0.07 | 0.00 | 0.34 | −0.55 | 0.00 |
| 0.528 | 121 | −0.90 | 0.22 | −1.84 | 1.06 | −1.94 | 5.92 |

*3.4.3 Shear deformation*. When a uniform strain $\varepsilon^0_{12}=\varepsilon^0_{21}$ is applied on the sample material boundary $S$, the periodic boundary conditions are written as

$$u_1(\underset{\sim}{x}+\underset{\sim}{L})=u_1(\underset{\sim}{x})+\varepsilon^0_{12}L\underset{\sim}{e}_2 \quad \text{on} \quad S \tag{31}$$

$$u_2(\underset{\sim}{x}+\underset{\sim}{L})=u_2(\underset{\sim}{x})+\varepsilon^0_{21}L\underset{\sim}{e}_1 \quad \text{on} \quad S \tag{32}$$

which gives $C^{\text{eff}}_{1212}=W^{\text{cell}}/2V$ when $\varepsilon^0_{12}=\varepsilon^0_{21}=1$.

## 4 Results

Effective and apparent elastic moduli of trabecular bone were studied computationally using the finite element software ANSYS, Version 8.1. In the 2D analysis we used solid elements (Quad 82 type) and a plane stress with thickness option. The analysis included four window sizes ($\delta=\delta_0$, $2\delta_0$, $3\delta_0$, and $6\delta_0$, where $\delta_0$ represents the size of a square unit cell shown in Figs. 2 and 3) and four types of boundary conditions: displacement, traction, mixed, and periodic. Other investigated parameters included the mesh size, the ratio of moduli of stiff bone tissue and soft material filling the pores, the sharp versus rounded corner geometry in the trabecular bone structure, and the bone tissue volume fraction. The Hill condition and average stress and average strain theorems were used to check the numerical results. A comparison between 2D and 3D models was also done. In all calculations, unless otherwise stated, we assumed the Young modulus of bone tissue $E_b$ =13 GPa, the mismatch in the bone tissue and soft tissue moduli $E_b/E_s=10^6$, the Poisson ratios $\nu_b=\nu_s=0.3$, and the volume fraction of the bone tissue equal to 20%.

**4.1 Effects of Mesh Size.** We conducted a parametric study to identify the optimum mesh size for analysis, namely, the smallest mesh that would minimize error and yet have a small number of elements. We considered the same and different mesh sizes for the stiff bone tissue making up the trabecular bone tissue network and the very soft material representing the pores. More specifically, we considered three different cases: the same uniform mesh size for both phases, bone tissue and soft fill, and the finer mesh for bone tissue or for soft phase. We applied traction and displacement boundary conditions and three different load types: uniaxial extension or tension, biaxial extension or tension, and shear deformation or shear traction. We varied finite element mesh sizes from crude (121 elements) to fine (12,996 elements). The Unit cell 1 model shown in Fig. 2(*a*) with a window size $\delta_0$ (see Fig. 3) was used in this parametric study. The unit cell had dimensions of 5 $\times 5\times 0.1$, and the mesh sizes ranged from 0.528 (crudest) to 0.044 (finest). The crudest mesh (0.528) represented the length of a finite element equal to the thickness $l$ of a strut in bone network (see Fig. 2), while the finest mesh (0.044) represented the $l/12$ finite element length. We conducted this investigation by comparing the elastic strain energies for those different cases with the elastic strain energies obtained using the finest mesh (0.044). We found that the configuration involving the same mesh sizes gave highest accuracy with fewer elements. The results for the same mesh size used for bone tissue and pores regions are given in Table 1, where $\Delta W(\%)=(W-W_f)/W\times 100\%$; $W$ denotes the elastic strain energy in a unit cell for a given mesh size and $W_f$ is the elastic strain energy obtained for the model with finest mesh. Based on these results we selected the same mesh size for bone tissue and soft tissue with 0.264 as the element length. This meant that we had two finite elements across the bone tissue strut. This mesh configuration gave accuracy within 1% for all loadings as compared with the finest mesh.

**4.2 Effects of Ratio of Moduli of Bone Tissue and Soft Fill.** In this section we investigate the effects of the moduli ratio $E_b/E_s$ on the apparent stiffness of our periodic model of bone. We set the modulus of the bone tissue as $E_b$=13 GPa and varied the fill material modulus $E_s$ from 1.3 Pa to 13 GPa to model a range of materials with stiff bone tissue and the variable bone fill. This allowed us to see how the choice of $E_s$ affected the results. The data are summarized in Fig. 4 for the displacement and traction boundary conditions cases. Note that the apparent stiffness components obtained using displacement and traction boundary conditions asymptote very quickly for lower mismatches, and they are nearly independent of the moduli ratio for the ratio greater than $10^2$; such result obtained using displacement boundary conditions

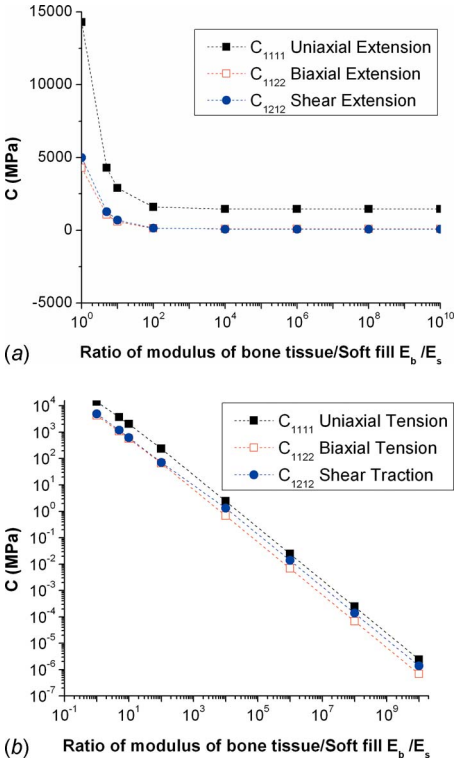


**Fig. 4 Apparent stiffness components as functions of $E_b/E_s$ ($E_b$=13 GPa, $\nu_b$=$\nu_s$=0.3, and bone tissue volume fraction 20%) (*a*) $C^d_{1111}$, $C^d_{1212}$, and $C^d_{1122}$; (*b*) $C^t_{1111}$, $C^t_{1212}$, and $C^t_{1122}$**

is shown in Fig. 4(*a*). The apparent stiffness components obtained using traction boundary conditions were plotted on a log-log scale to illustrate the small changes in stiffness components for large mismatches. These results plotted on the log-log scale show a linear trend (Fig. 4(*b*)). Thus, the actual value of the soft fill modulus used in our analysis had little influence on our results when the mismatch is larger than $10^2$. This parametric study also illustrated that the results converged for the whole range of elastic moduli mismatches.

**4.3 Effects of Sample Window Size and Boundary Conditions.** The periodic model of trabecular bone was represented by repeating unit cells (Fig. 3). We used Unit cell 1 (Fig. 2(*a*)) as a repeating unit, assumed a volume fraction of 20% and took four different window sizes ($\delta=\delta_0$, $2\delta_0$, $3\delta_0$, and $6\delta_0$). We applied displacement, traction, and mixed boundary conditions involving uniaxial, biaxial, and shear loadings to obtain the apparent elastic moduli and periodic boundary conditions to obtain the effective elastic moduli. We obtained $C^d_{ijkl}$, $C^{dt}_{ijkl}$, and $C_{ijkl}$ using displacement, mixed, and periodic boundary conditions, respectively, and $C^t_{ijkl}=(S^t_{ijkl})^{-1}$ using traction boundary conditions.

We illustrate the apparent and effective stiffness tensor components, $C_{1111}$, $C_{1122}$, and $C_{1212}$, obtained using the above mentioned four boundary conditions in Fig. 5. Results obtained using periodic boundary conditions gave the effective stiffness, and they were independent of window size. Note that the apparent stiffness components $C_{1111}$ and $C_{1212}$ obtained using displacement boundary conditions bound the effective properties from above, while those obtained using traction boundary conditions bound the effective properties from below, as predicted by Eq. (1), and these bounds are very wide. The results obtained using mixed boundary conditions fall between these two bounds as predicted by Eq. (2). The results obtained using mixed boundary conditions are very close to those obtained using the effective properties. Also, the results for $C^d_{1111}$, obtained using displacement boundary conditions, are closer to the effective ones that those obtained using traction boundary conditions, while the results for $C^t_{1212}$ are closer to the effective one than those obtained using displacement boundary conditions. It is interesting to observe that, in general, the stiffness components obtained using displacement and traction boundary conditions are not very sensitive to the increasing window size, and these bounds converge very slowly and are still very wide for the case of $6\delta_0$, in particular, for $C_{1111}$. The $C^d_{1122}$ and $C^d_{1212}$, obtained using displacement boundary conditions, show higher sensitivity to the window size.

**4.4 The Comparison Between Two Types of Unit Cells.** The choice of a unit cell is not unique for our periodic model. We considered two different unit cells, as shown in Fig. 2. Unit cell 1 (Fig. 2(*a*)) has bone tissue in the crosslike shape in the central part of the cell with soft material present on its outer edges, while Unit cell 2 (Fig. 2(*b*)) has the bone tissue present on its boundary, which fully encloses the soft fill. For this choice of unit cell only the bone tissue is present on the boundary. We studied the effect of these two types of unit cells by applying displacement and traction boundary conditions. Note that the results obtained using Unit cell 2 gave, in general, closer bounds than those obtained for Unit cell 1, as seen in Fig. 6.

**4.5 The Effects of Sharp-Corners in the Trabecular Bone Geometry.** In this paper we modeled the bone structure, for simplicity, as having square pores with sharp corners. The actual bone structure has rounded corners. These sharp corners can serve as stress concentrators. Thus, we investigated the effect of sharp corner versus rounded corner geometry on the apparent and effective moduli by comparing the results obtained using the model with sharp corners (Fig. 2(*a*)) and the model with rounded corners (Fig. 7). The rounded corner geometry had $l=0.5$ and the radius of curvature $r=0.5$. The results are given in Table 2 for the case of displacement and traction boundary conditions. Note that for the

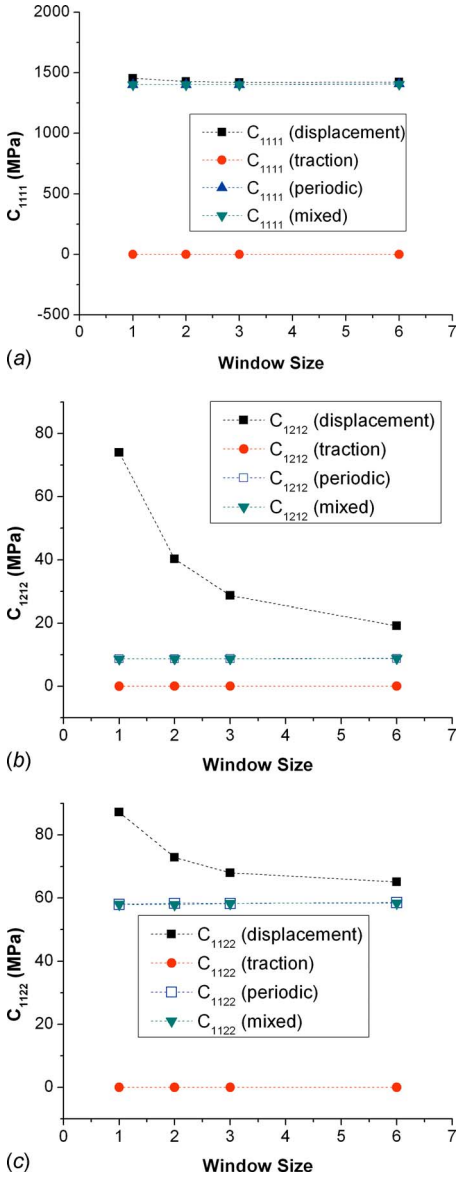


**Fig. 5 Comparison of the apparent elastic stiffness components (*a*) $C^{app}_{1111}$, (*b*) $C^{app}_{1212}$, and $C^{app}_{1122}$ obtained using displacement, traction, and mixed boundary conditions, and the effective elastic stiffness components obtained using periodic boundary conditions (Unit cell 1 was used)**

stiffness component $C^d_{1111}$ obtained using displacement boundary conditions and for all components obtained using traction boundary conditions there is no significant difference (~1%) between these two models. The stiffness components $C^d_{1122}$ and $C^d_{1212}$ are most affected. In all cases, the stiffness components for the model with sharp corners are lower than those for the geometry with rounded corners.

**4.6 The Effects of Bone Volume Fractions.** Volume fraction of bone tissue is an important parameter describing the trabecular structure and influencing its mechanical properties. For example, osteoporosis is characterized by higher porosity of bone. In order to illustrate the effect of the volume fraction of bone tissue on apparent stiffness, we considered three volume fractions of bone tissue: 5%, 10%, and 20%. The apparent elastic stiffness components $C^{app}_{1111}$, $C^{app}_{1122}$, and $C^{app}_{1212}$ were obtained using displacement and traction boundary conditions for four different window sizes ($\delta=\delta_0$, $2\delta_0$, $3\delta_0$, and $6\delta_0$) using Unit cell 1. The results are given

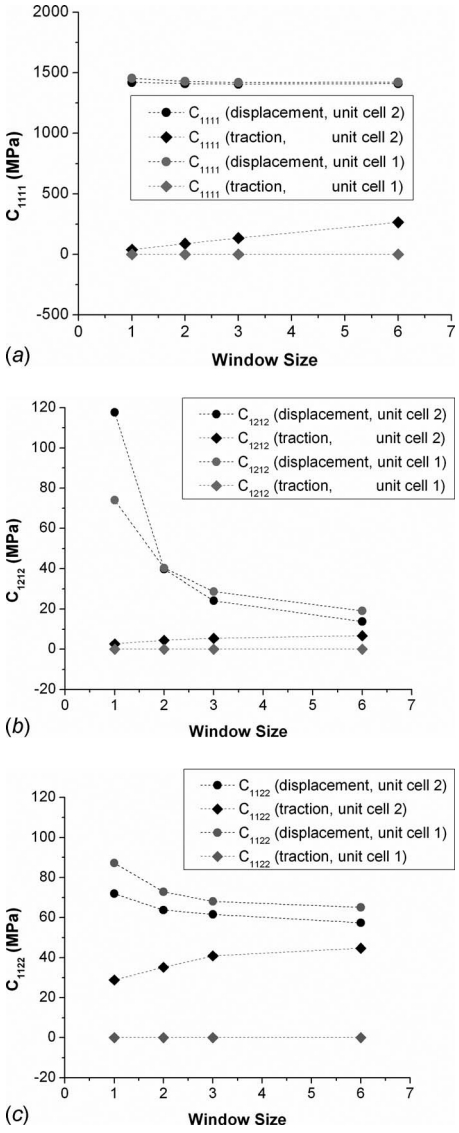


**Fig. 6 Comparison of the apparent elastic stiffness components (*a*) $C^{app}_{1111}$, (*b*) $C^{app}_{1212}$, and (*c*) $C^{app}_{1122}$ obtained using Unit cells 1 and 2 and displacement and traction boundary conditions**

in Fig. 8. The following observations can be made about the apparent stiffness components $C_{1111}$, $C_{1122}$, and $C_{1212}$. They all increase with the increasing bone tissue volume fraction, as expected. This increase is nearly linear for all three stiffness components for each boundary condition, except for $C^d_{1212}$ and

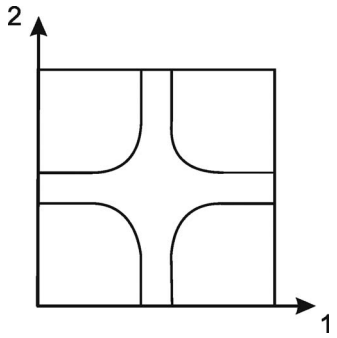


**Fig. 7 Unit cell of idealized periodic model of trabecular bone without sharp corners**

$C^d_{1122}$ obtained using displacement boundary conditions. The changes in the elastic moduli under displacement boundary conditions are larger than those in the elastic moduli under traction boundary conditions. It is interesting to observe that the stiffness components obtained using displacement boundary conditions are higher for smaller window sizes, while the opposite trend is observed for the stiffness components obtained using traction boundary conditions. Finally, the stiffness components obtained using displacement boundary conditions are insensitive to the window size for the 5% volume fraction.

**4.7 The Comparison of 2D and 3D Models With the Same Bone Volume Fraction.** In this paper we focused on the 2D geometry for computational simplicity. In this section we compare the 2D versus 3D geometry in order to show a relation of our 2D results to 3D results. Recall that our 2D model involved a plane stress assumption with thickness. We constructed our 3D model (Fig. 9) by using the analogous structure to our 2D model, with the same bone tissue volume fraction (20%) and same elastic properties of constituents as in the 2D model ($E_b$=13 GPa, $E_b/E_s=10^6$, and $\nu_b=\nu_s=0.3$). We applied displacement and traction boundary conditions to evaluate the apparent stiffness components. The results compared with those of 2D model are shown in Fig. 10. It is interesting to note that the apparent 2D and 3D stiffness components obtained using traction boundary conditions are very close to each other, while the ones obtained using displacement boundary conditions show a larger difference. The $C^d_{1111}$ component is higher for the 2D case, while the $C^d_{1212}$ prediction is higher for the 3D case.

**4.8 The Hill condition, Average Stress Theorem, and Average Strain Theorems.** We also checked if the Hill condition and the average stress or strain theorems are satisfied. The calculations were done for the case when $E_b$=13 GPa, $E_b/E_s=10^6$, $\nu_b=\nu_s$ =0.3, and 20% volume fraction of bone tissue. Three types of loadings (uniaxial extension or tension, biaxial extension or tension, and shear deformation or shear traction) were considered for each type of boundary conditions (displacement, traction, mixed, and periodic)). We observed that the Hill condition was satisfied for all four types of boundary conditions and for each loading case, as expected. Note that the satisfaction of the Hill condition would not be possible if the fill material would remain a void with stiffness components being identically zero. We also checked the average strain $\overline{\varepsilon_{ij}}$ and average stress $\overline{\sigma_{ij}}$ components for each boundary condition and each loading. The average stress theorem was satisfied for the case of traction and mixed boundary conditions, and the average strain theorem was satisfied for the cases of displacement, periodic and mixed boundary conditions.

## 5 Discussion

In this paper we represented trabecular bone by using a very simple periodic geometric model with repeating unit cells (Fig. 2), even though trabecular bone has a very complex random architecture. We made this assumption for simplicity so we could focus on the effects of scale and boundary conditions and not on the complexity of bone's architecture. If a trabecular bone were represented as a material with random structure we would need to consider a large number of realizations and the analysis would require much more computer power. Such problem was addressed by us in Ref. [54] in the context of composite materials. The trends were similar as for the periodic case [67,68]. Pahr and Zysset [51] studied the effect of boundary conditions on the computed apparent elastic properties of trabecular bone by considering realistic trabecular bone structures taken from six human bone samples. However, as commented by the authors, this number of realizations was not sufficient to predict the overall elastic properties of trabecular bone.

**5.1 Effect of Mesh Size.** Since our objective was in studying scale effects, we were interested in being able to build the largest

**Table 2 Comparison of the apparent stiffness components $C_{1111}$, $C_{1122}$, and $C_{1212}$ for rounded versus sharp corner geometry when $E_b$=13 GPa, $E_b/E_s=10^6$, $\nu_b=\nu_s$=0.3, and bone tissue volume fraction 20%**

| Model | $C^d_{1111}$ (MPa) | $C^t_{1111}$ (MPa) | $C^d_{1122}$ (MPa) | $C^t_{1122}$ (MPa) | $C^d_{1212}$ (MPa) | $C^t_{1212}$ (MPa) |
|---|---|---|---|---|---|---|
| Rounded corners | $1.46\times10^3$ | $2.42\times10^{-1}$ | 101.2 | $0.68\times10^{-2}$ | 81.2 | $1.38\times10^{-2}$ |
| Sharp corners | $1.45\times10^3$ | $2.39\times10^{-2}$ | 87.2 | $0.68\times10^{-2}$ | 74.0 | $1.36\times10^{-2}$ |

systems possible with the available computer resources. We found that the same mesh size for bone tissue and bone fill gave the best convergence. Two elements across the strut gave the 1% accuracy for all loadings (Table 1). Our study can be extended, using more powerful computers, by considering finer meshes and larger window sizes.

**5.2 Effects of Ratio of Moduli of Bone Tissue and Soft Fill.** In this paper we modeled the bone tissue and soft fill as homogeneous, linear elastic, and isotropic for simplicity. This is a common assumption used in bone literature for trabecular bone studies. Strictly speaking bone is viscoelastic, inhomogeneous, and locally anisotropic. In this paper we assumed Young's moduli $E_b$=13 GPa and $E_s$=13 kPa and Poisson's ratios $\nu_b=\nu_s$=0.3. The property of bone tissue was selected from a variety of values taken from literature. The very small value of $E_b$ makes this problem equivalent to the case when soft fill is not present, i.e., the space is filled by voids. Such assumption has been used in most computational studies on trabecular bone. However, we needed to include the fill in our model to ensure that the average stress and strain theorems and the Hill condition were satisfied. We explored the effect of soft fill modulus by considering a range of values (from $E_s$=1.3 Pa to 13 GPa) for the following reasons. We were most interested in the fill material having very low moduli but considered a range of values to check convergence of results up to the mismatch of $E_b/E_s=10^9$. Also, we wanted to see how our choice of soft fill material properties has influenced our results. In our analysis we assumed that the Poisson's ratio of the soft fill is 0.3. We also considered the case of $\nu_s$=0.5 to simulate the case of a very soft tissue or a fluid. The results were almost the same as for the $\nu_s$=0.3 case for all stiffness components $C^d_{1111}$, $C^d_{1122}$, and

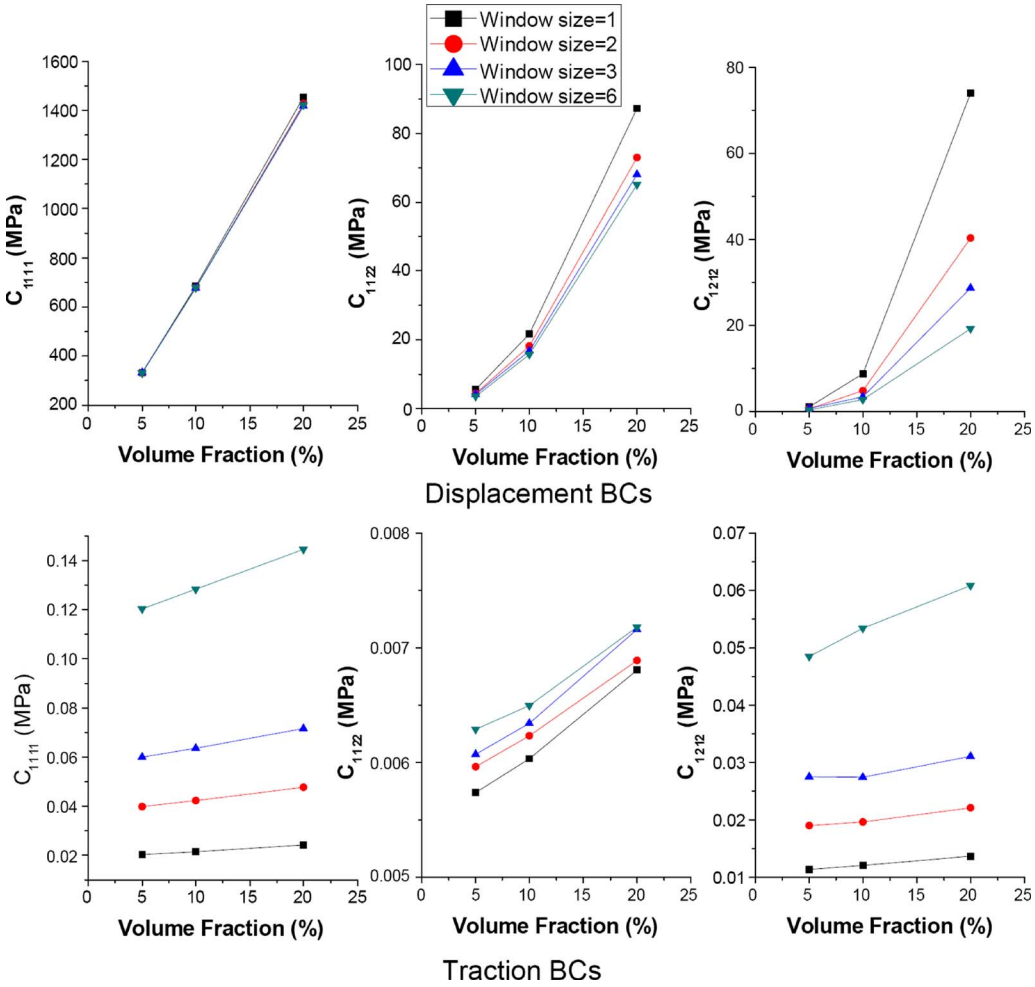


**Fig. 8 Comparison of the apparent elastic stiffness components $C^{app}_{1111}$, $C^{app}_{1122}$ and $C^{app}_{1212}$, obtained using three different volume fractions (5%, 10%, and 20%) and displacement and traction boundary conditions, for four different window sizes ($\delta=\delta_0$, $2\delta_0$, $3\delta_0$, and $6\delta_0$) using Unit cell 1**

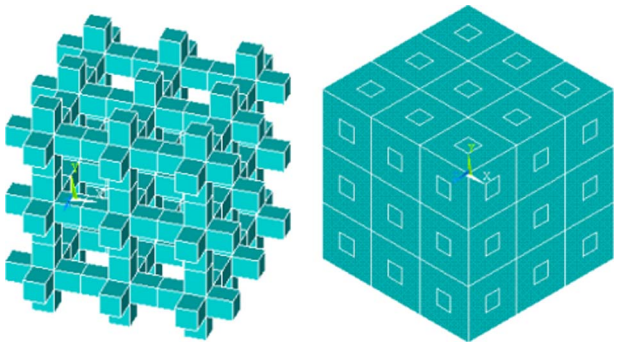

**Fig. 9 The 3D periodic model of trabecular bone with 3×3 ×3 unit cells for 20% bone tissue volume fraction**

$C^d_{1212}$ obtained using displacement boundary loading and for $C^t_{1111}$ and $C^t_{1212}$. However, the results differed by nearly 50% for the case of $C^t_{1122}$ with the case of $\nu_s$=0.5 being higher.

**5.3 Effects of Sample Window Size and Boundary Conditions.** Effective moduli were obtained applying periodic boundary conditions, and they were independent of the window size, as expected. The idea of periodic boundary conditions is that when applied to a periodic structure, they simulate the overall response of a material having a periodic and repeating structure. The apparent stiffness components $C_{1111}$ and $C_{1212}$ obtained using displacement and traction boundary conditions gave upper and lower bounds, respectively, on the effective elastic properties, as expected from the results of Hollister and Kikuchi [57], Huet [47], and Eq. (1). Note that the Eq. (1), written for tensor quantities, applies to the stiffness components, $C_{1111}$ and $C_{1212}$, but not to $C_{1122}$. The apparent moduli $C_{1111}$ and $C_{1212}$ obtained using mixed

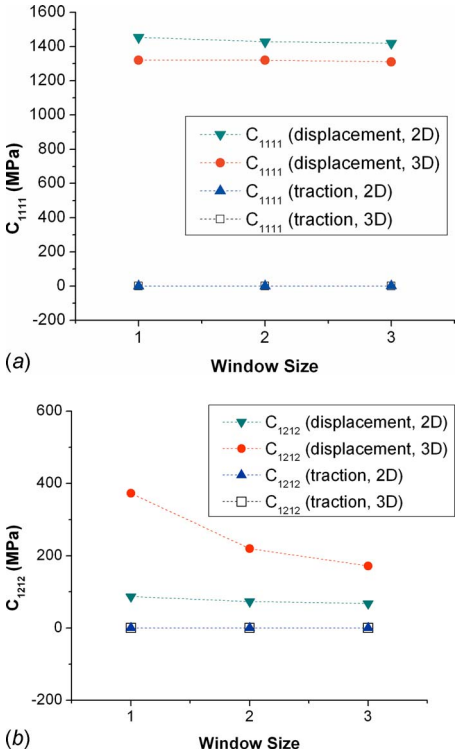


**Fig. 10 Comparison of the apparent elastic stiffness components (*a*) $C^{app}_{1111}$ and (*b*) $C^{app}_{1212}$ for two dimensions and three dimensions obtained using displacement and traction boundary conditions and Unit cell 1**

boundary conditions fell between these two bounds, as expected from Eq. (2). The results using mixed boundary conditions were very close to the effective properties. This is in agreement with our earlier results on the scale and boundary conditions effects in composite materials [67]. Note that the results obtained using displacement boundary conditions were closer to the effective ones than those obtained using traction boundary conditions. The apparent elastic moduli obtained using displacement and traction boundary conditions were, in general, not sensitive to the increasing window size, and these bounds converged very slowly because of a large mismatch in elastic moduli. This result is consistent with our earlier results on composite materials with large mismatches (e.g., Ref. [54]). The results for $C^d_{1212}$ and $C^d_{1212}$ obtained using displacement boundary conditions showed higher sensitivity to window size. The general trends on the effects of scale and boundary conditions (displacement and traction) obtained by us are similar to those obtained by Hollister and Kikuchi [57] for similar geometries (periodic composites with circular pores).

**5.4 The Comparisons of Two Types of Unit Cells.** For our periodic model the choice of a unit cell is not unique. We considered two different choices (Fig. 2). The choice of unit cell is not important for the case of periodic boundary conditions, and results are the same for these two unit cells, as expected. When we applied displacement or traction boundary conditions, the results obtained using Unit cell 2 gave, in general, closer bounds than those obtained for Unit cell 1. This is expected because for the Unit cell 2 case, the deformations on the edges due to displacement and traction boundary conditions are closer to each other than those obtained for Unit cell 1. In the case of Unit cell 1 the deformation due to traction boundary conditions differs more from the one obtained using displacement boundary conditions because the soft tissue deforms more in that case. This result gives guidance on how to choose a unit cell for computations to minimize the effect of boundary conditions. Thus, a better convergence of bounds in obtained when the inclusions are fully enclosed within a matrix. One usually has such a choice for periodic structures but not for random ones. Thus, in the case of random geometries, such as in trabecular bone, the inclusions (in this case pores) will usually be crossed by the boundary which will amplify the boundary conditions effects.

**5.5 The Effects of Sharp-Corners in Modeling Trabecular Bone Geometry.** We compared two different geometries, with sharp corners (Fig. 2(*a*)) and with rounded corners (Fig. 7). We found no significant difference between these two models except for the case of $C^d_{1212}$ and $C^d_{1122}$. We studied the effect of sharp versus rounded corners on effective elastic moduli in Ref. [71], where inclusions with different polygonal shapes and different degrees of sharpness at corners were considered. In that study we found that materials with voids with sharper corners had lower effective Young's moduli than materials with rounded corners due to higher stress concentrations in the case of sharp corners. Our results for $C_{1111}$, $C_{1122}$, and $C_{1212}$ follow this trend.

**5.6 The Effects of Bone Volume Fractions.** We found that all stiffness components increased with the increasing bone tissue volume fractions, as expected (Fig. 6). The larger the amount of tissue is, the higher is the modulus for the same geometry, as expected. The stiffness components $C_{1111}$, $C_{1122}$, and $C_{1212}$ showed, in general, a linear dependence on volume fraction. This is in agreement with results of Christensen [14] and Gibson and Ashby [13].

**5.7 The Comparison of 2D and 3D Models Under the Same Bone Volume Fraction.** The results for two dimensions and three dimensions were comparable, and the trends observed for 2D case carry over qualitatively to 3D geometry.

**5.8 The Hill Condition, Average Stress Theorem, and Average Strain Theorems.** The Hill condition and average stress and strain theorems were satisfied. These ensure the accuracy and uniqueness of results. Special care is required to model materials with voids. The presence of fill material, even though very soft, needs to be included to satisfy the above conditions.

## 6 Conclusions

We studied the effective and apparent elastic properties of trabecular bone represented by an idealized periodic structure. Effective elastic properties were found by applying periodic boundary conditions, while the apparent elastic properties were found by applying displacement, traction, or mixed boundary conditions. The results depended on the window size, boundary conditions, and different unit cell choices. Results using displacement and traction boundary conditions gave wide bounds, which converged very slowly with increasing window sizes.

This study was motivated by the fact that only a limited amount of bone tissue is available for testing because of the finite bone size and spatially changing porosity. Thus, in general, the apparent properties are obtained, which are dependent on specimen size and boundary conditions. This study focused on this dependence for simple periodic geometries. These results can give guidance on how the specimen size and applied boundary conditions affect elastic moduli of cellular materials. Our findings can also give guidance on the response of trabecular bone with actual 3D random structures.

## Acknowledgment

This research was supported by Natural Sciences and Engineering Research Council (NSERC) of Canada and the National Science Foundation (CMMI 09-27909 ARRA, Dr. Ken Chong).

## References

[1] Hollister, S. J., Brennan, J. M., and Kikuchi, N., 1994, "A Homogenization Sampling Procedure for Calculating Trabecular Bone Effective Stiffness and Tissue Level Stress," J. Biomech., **27**, pp. 433–444.
[2] van Rietbergen, B., Weinans, H., Huiskes, R., and Odgaard, A., 1995, "A New Method to Determine Trabecular Bone Elastic Properties and Loading Using Micromechanical Finite-Element Models," J. Biomech., **28**, pp. 69–81.
[3] van Rietbergen, B., Odgaard, A., Kabel, J., and Huiskes, R., 1996, "Direct Mechanics Assessment of Elastic Symmetries and Properties of Trabecular Bone Architecture," J. Biomech., **29**, pp. 1653–1657.
[4] van Rietbergen, B., Odgaard, A., Kabel, J., and Huiskes, R., 1998, "Relationships Between Bone Morphology and Bone Elastic Properties Can Be Accurately Quantified Using High-Resolution Computer Reconstructions," J. Orthop. Res., **16**, pp. 23–28.
[5] Niebur, G. L., Yuen, J. C., Hsia, A. C., and Keaveny, T. M., 1999, "Convergence Behavior of High-Resolution Finite Element Models of Trabecular Bone," ASME J. Biomed. Eng., **121**, pp. 629–635.
[6] Niebur, G. L., Feldstein, M. J., Yuen, J. C., and Keaveny, T. M., 2000, "High Resolution Finite Element Models With Tissue Strength Asymmetry Predict Failure of Trabecular Bone," J. Biomech., **33**, pp. 1575–1583.
[7] Pistoia, W., van Rietbergen, B., Laib, A., and Ruegsegger, P., 2001, "High Resolution Three-Dimensional-pQCT Images Can Be an Adequate Basis for In-Vitro MicroFE Analysis of Bone," ASME J. Biomech. Eng., **123**, pp. 176–183.
[8] van Lenthe, G. H., Stauber, M., and Muller, R., 2006, "Specimen-Specific Beam Models for Fast and Accurate Prediction of Human Trabecular Bone Mechanical Properties," Bone, **39**, pp. 1182–1189.
[9] Silva, M. J., Hayes, W. C., and Gibson, L. J., 1995, "The Effects of Non-Periodic Microstructure on the Elastic Properties of Two-Dimensional Cellular Solids," Int. J. Mech. Sci., **37**, pp. 1161–1177.
[10] Silva, M. J., and Gibson, L. J., 1997, "Modeling the Mechanical Behavior of Vertebral Trabecular Bone: Effects of Age-Related Changes in Microstructure," Bone, **21**, pp. 191–199.
[11] Ashby, M. F., 1983, "The Mechanical Properties of Cellular Solids," Metall. Mater. Trans. A, **14**, pp. 1755–1769.
[12] Gibson, L., 1985, "The Mechanical Behaviour of Cancellous Bone," J. Biomech., **18**, pp. 317–328.
[13] Gibson, L. J., and Ashby, M. F., 1988, *Cellular Solids: Structure and Properties*, Pergamon, Oxford, England.
[14] Christensen, R. M., 1986, "Mechanics of Low Density Materials," J. Mech. Phys. Solids, **34**, pp. 563–578.
[15] Williams, J. L., and Lewis, J. L., 1982, "Properties and an Anisotropic Model of Cancellous Bone From the Proximal Tibia Epiphysis," ASME J. Biomech. Eng., **104**, pp. 50–56.
[16] Beaupre, G. S., and Hayes, W. C., 1985, "Finite Element Analysis of a Three-Dimensional Open-Celled Model for Trabecular Bone," ASME J. Biomech. Eng., **107**, pp. 249–256.
[17] Hollister, S. J., Fyhrie, D. P., Jepsen, K. J., and Goldstein, S. A., 1991, "Application of Homogenization Theory to the Study of Trabecular Bone Mechanics," J. Biomech., **24**, pp. 825–839.
[18] Guo, X.-D. E., McMahon, T. A., Keaveny, T. M., Hayes, W. C., and Gibson, L. J., 1994, "Finite Element Modeling of Damage Accumulation in Trabecular Bone Under Cyclic Loading," J. Biomech., **27**, pp. 145–155.
[19] Werner, H. J., Matin, H., Behrend, D., Schmitz, K. P., and Schober, H. C., 1996, "The Loss of Stiffness as Osteoporosis Progresses," Med. Eng. Phys., **18**, pp. 601–606.
[20] Kowalczyk, P., 2003, "Elastic Properties of Cancellous Bone Derived From Finite Element Models of Parameterized Microstructure Cells," J. Biomech., **36**, pp. 961–972.
[21] Adachi, T., Tomita, Y., and Tanaka, M., 1998, "Computational Simulation of Deformation Behavior of 2D-Lattice Continuum," Int. J. Mech. Sci., **40**, pp. 857–866.
[22] Bouyge, F., Jasiuk, I., and Ostoja-Starzewski, M., 2001, "A Micromechanically Based Couple-Stress Model of an Elastic Two-Phase Composite," Int. J. Solids Struct., **38**, pp. 1721–1735.
[23] Bouyge, F., Jasiuk, I., Boccara, S., and Ostoja-Starzewski, M., 2002, "A Micromechanically Based Couple-Stress Model of an Elastic Orthotropic Two-Phase Composite," Eur. J. Mech. A/Solids, **21**, pp. 465–481.
[24] Fatemi, J., van Keulen, F., and Onck, P. R., 2002, "Generalized Continuum Theories: Application to Stress Analysis in Bone," Meccanica, **37**, pp. 385–396.
[25] Fatemi, J., Onck, P. R., Poort, G., and van Keulen, F., 2003, "Cosserat Moduli of Anisotropic Cancellous Bone: A Micromechanical Analysis," J. Phys. IV, **105**, pp. 273–280.
[26] Tekoglu, C., and Onck, P. R., 2003, "A Comparison of Discrete and Cosserat Continuum Analyses for Cellular Materials," *Proceedings of MetFoam 2003, Cellular Metals: Manufacture, Properties, Applications*, J. Banhart, N. A. Fleck, and A. Mortensen, eds., MIT, Berlin, p. 339.
[27] Yoo, A., and Jasiuk, I., 2006, "Couple-Stress Moduli of a Trabecular Bone Idealized as a 3D Periodic Cellular Network," J. Biomech., **39**, pp. 2241–2252.
[28] Yang, J. F. C., and Lakes, R. S., 1982, "Experimental Study of Micropolar and Couple Stress Elasticity in Bone in Bending," J. Biomech., **15**, pp. 91–98.
[29] Park, H. C., and Lakes, R. S., 1986, "Cosserat Micromechanics of Human Bone: Strain Redistribution by a Hydration-Sensitive Constituent," J. Biomech., **19**, pp. 385–397.
[30] Park, H. C., and Lakes, R. S., 1987, "Torsion of a Micropolar Elastic Prism of Square Cross Section," Int. J. Solids Struct., **23**, pp. 485–503.
[31] Lakes, R., 1982, "Dynamical Study of Couple-Stress Effects in Human Compact Bone," ASME J. Biomech. Eng., **104**, pp. 6–11.
[32] Lakes, R. S., 1995, "Experimental Methods for Study of Cosserat Elastic Solids and Other Generalized Elastic Continua," *Continuum Models for Materials With Micro-Structure*, H. Muhlhaus, ed., Wiley, New York.
[33] Bonifasi-Lista, C., and Cherkaev, E., 2008, "Analytical Relations Between Effective Material Properties and Microporosity: Application to Bone Mechanics," Int. J. Eng. Sci., **46**, pp. 1239–1252.
[34] Cowin, S. C., 1999, "Bone Poroelasticity," J. Biomech., **32**, pp. 217–238.
[35] Turner, C. H., Cowin, S. C., Rho, J. Y., Ashman, R. B., and Rice, J. C., 1990, "The Fabric Dependence of the Orthotropic Elastic Constants of Cancellous Bone," J. Biomech., **23**, pp. 549–561.
[36] Yang, G., Kabel, J., Van Rietbergen, B., Odgaard, A., Huiskes, R., and Cowin, S. C., 1998, "The Anisotropic Hooke's Law for Cancellous Bone and Wood," J. Elast., **53**, pp. 125–146.
[37] Zysset, P. K., 2003, "A Review Of Morphology-Elasticity Relationships in Human Trabecular Bone: Theories and Experiments," J. Biomech., **36**, pp. 1469–1485.
[38] Jaasma, M. J., Bayraktar, H. H., Neibur, G. L., and Keaveny, T. M., 2002, "Biomechanical Effects of Intraspecimen Variations in Tissue Modulus for Trabecular Bone," J. Biomech., **35**, pp. 237–246.
[39] Tai, K., Dao, M., Suresh, S., Palazoglu, A., and Ortiz, C., 2007, "Nanoscale Heterogeneity Promotes Energy Dissipation in Bone," Nature Materials, **6**, pp. 454–462.
[40] Biot, M. A., 1941, "General Theory of Three-Dimensional Consolidation," J. Appl. Phys., **12**, pp. 155–164.
[41] Hill, R., 1963, "Elastic Properties of Reinforced Solids: Some Theoretical Considerations," J. Mech. Phys. Solids, **11**, pp. 357–372.
[42] Hashin, Z., 1983, "Analysis of Composite Materials," ASME J. Appl. Mech., **50**, pp. 481–505.
[43] Aboudi, J., 1991, *Mechanics of Composite Materials—A Unified Micromechanical Approach*, Elsevier, New York.
[44] Christensen, R. M., 1979, *Mechanics of Composite Materials*, Wiley, New York.
[45] Ostoja-Starzewski, M., 2006, "Material Spatial Randomness—From Statistical to Representative Volume Element," Probab. Eng. Mech., **21**, pp. 112–132.
[46] Ostoja-Starzewski, M., 2008, *Microstructural Randomness and Scaling in Mechanics of Materials*, Chapman & Hall/CRC/Taylor & Francis, Boca Raton, FL, USA.
[47] Huet, C., 1990, "Application of Variational Concepts to Size Effects in Elastic Heterogeneous Bodies," J. Mech. Phys. Solids, **38**, pp. 813–841.
[48] Hazanov, S., and Huet, C., 1994, "Order Relationships for Boundary Conditions Effect in Heterogeneous Bodies Smaller Than Representative Volume," J.

Mech. Phys. Solids, **42**, pp. 1995–2011.
[49] Hazanov, S., and Amieur, M., 1995, "On Overall Properties of Elastic Heterogeneous Bodies Smaller Than the Representative Volume," Int. J. Eng. Sci., **33**, pp. 1289–1301.
[50] Hazanov, S., 1998, "Hill Condition and Overall Properties of Composites," Arch. Appl. Mech., **68**, pp. 385–394.
[51] Pahr, D. H., and Zysset, P. K., 2008, "Influence of Boundary Conditions on Computed Apparent Elastic Properties of Cancelous Bone," Biomech. Model. Mechanobiol., **7**, pp. 463–476.
[52] Ostoja-Starzewski, M., 1999, "Scale Effects in Materials With Random Distributions of Needles and Cracks," Mech. Mater., **31**, pp. 883–893.
[53] Pecullan, S., Gibiansky, L. V., and Torquato, S., 1999, "Scale Effects on the Elastic Behavior of Periodic and Hierarchical Two-Dimensional Composites," J. Mech. Phys. Solids, **47**, pp. 1509–1542.
[54] Jiang, M., Alzebdeh, K., Jasiuk, I., and Ostoja-Starzewski, M., 2001, "Scale and Boundary Conditions Effects in Elastic Properties of Random Composites," Acta Mech., **148**, pp. 63–78.
[55] Ostoja-Starzewski, M., Du, X., Khisaeva, Z. F., and Li, W., 2007, "Comparisons of the Size of Representative Volume Element in Elastic, Plastic, Thermoelastic, and Permeable Random Microstructures," Int. J. Multiscale Comp. Eng., **5**, pp. 73–82.
[56] Ranganathan, S. I., and Ostoja-Starzewski, M., 2008, "Scaling Function, Anisotropy and the Size of RVE in Elastic Random Polycrystals," J. Mech. Phys. Solids, **56**, pp. 2773–2791.
[57] Hollister, S. J., and Kikuchi, N., 1992, "A Comparison of Homogenization and Standard Mechanics Analyses for Periodic Porous Composites," Comput. Mech., **10**, pp. 73–95.
[58] Harrigan, T. P., Jasty, M., Mann, R. W., and Harris, W. H., 1988, "Limitations of the Continuum Assumption in Cancellous Bone," J. Biomech., **21**, pp. 269–275.
[59] Linde, F., and Hvid, I., 1989, "The Effect of Constraint on the Mechanical Behaviour of Trabecular Bone Specimens," J. Biomech., **22**, pp. 485–490.
[60] Choi, K., Kuhn, J. L., Ciarelli, M. J., and Goldstein, S. A., 1990, "The Elastic Moduli of Human Subchondral, Trabecular, and Cortical Bone Tissue and the Size-Dependency of Cortical Bone Modulus," J. Biomech., **23**, pp. 1103–1113.
[61] Odgaard, A., and Linde, F., 1991, "The Underestimation of Young's Modulus in Compressive Testing of Cancellous Bone Specimens," J. Biomech., **24**, pp. 691–698.
[62] Linde, F., Hvid, I., and Madsen, F., 1992, "The Effect of Specimen Geometry on the Mechanical Behaviour of Trabecular Bone Specimens," J. Biomech., **25**, pp. 359–368.
[63] Keaveny, T. M., Borchers, R. E., Gibson, L. J., and Hayes, W. C., 1993, "Trabecular Bone Modulus and Strength Can Depend on Specimen Geometry," J. Biomech., **26**, pp. 991–1000.
[64] Zhu, M., Keller, T. S., and Spengler, D. M., 1994, "Effects Of Specimen Load-Bearing and Free Surface Layers on the Compressive Mechanical Properties of Cellular Materials," J. Biomech., **27**, pp. 57–66.
[65] Jacobs, C. R., Davis, B. R., Rieger, C. J., Francis, J. J., Saad, M., and Fyhrie, D. P., 1999, "The Impact of Boundary Conditions and Mesh Size on the Accuracy of Cancellous Bone Tissue Modulus Determination Using Large-Scale Finite-Element Modeling," J. Biomech., **32**, pp. 1159–1164.
[66] Un, K., Bevill, G., and Keaveny, T. M., 2006, "The Effects of Side-Artifacts on the Elastic Modulus of Trabecular Bone," J. Biomech., **39**, pp. 1955–1963.
[67] Jiang, M., Jasiuk, I., and Ostoja-Starzewski, M., 2002, "Apparent Elastic and Elastoplastic Behavior of Periodic Composites," Int. J. Solids Struct., **39**, pp. 199–212.
[68] Jiang, M., Jasiuk, I., and Ostoja-Starzewski, M., 2002b, "Apparent Thermal Conductivity of Periodic Two-Dimensional Composites," Comput. Mater. Sci., **25**, pp. 329–338.
[69] Rho, J. Y., Tsui, T. Y., and Pharr, G. M., 1997, "Elastic Properties of Human Cortical and Trabecular Lamellar Bone Measured by Nanoindentation," Biomaterials, **18**, pp. 1325–1330.
[70] Zysset, P. K., Guo, X. E., Hoffler, C. E., Moore, K. E., and Goldstein, S. A., 1999, "Elastic Modulus and Hardness of Cortical and Trabecular Bone Lamellae Measured by Nanoindentation in the Human Femur," J. Biomech., **32**, pp. 1005–1012.
[71] Jasiuk, I., 1995, "Cavities Vis-À-Vis Rigid Inclusions: Elastic Moduli of Materials With Polygonal Inclusions," Int. J. Solids Struct., **32**, pp. 407–422.